SUPPLEMENTARY MATERIAL: EXPERIMENTAL DEMONSTRATION OF A PLASTIC SELF-ADAPTING INTEGRATED PHOTONIC NEURAL NETWORK

Alessio Lugnan
Photonics Research Group
Ghent University - imec
Ghent 9052, Belgium
alessio.lugnan.1@unitn.it

Samarth Aggarwal
Department of Materials
University of Oxford
Parks Road, Oxford OX1 3PH, UK

Frank Brückerhoff-Plückelmann
Department of Physics, CeNTech
University of Münster
Heisenbergstraße 11, 48149 Münster, Germany

C. David Wright
Department of Engineering
University of Exeter
Exeter EX4 4QF, UK

Wolfram H. P. Pernice
Department of Physics, CeNTech
University of Münster
Heisenbergstraße 11, 48149 Münster, Germany

Harish Bhaskaran
Department of Materials
University of Oxford
Parks Road, Oxford OX1 3PH, UK

Peter Bienstman
Photonics Research Group
Ghent University - imec
Ghent 9052, Belgium

1 Characterization of a single plastic node

In this supplementary section we present the experimental characterization of an integrated plastic node, namely a silicon microring resonator (MRR) with phase change material (PCM) cell (see Fig. 1 a, b), which was used as a building block in photonic plastic networks discussed in the main text. A MRR is resonant only to wavelengths that can fit an integer number of times along the ring waveguide, so that the light travelling in the ring interferes constructively with itself after a round trip. If this condition is met, the input light accumulates in the ring and part of it is redirected to the *drop* port. Otherwise, for wavelengths far from the resonant condition, most of the input signal continues its travel along the straight waveguide (to the *through* port), approximately undisturbed by the presence of the resonator (see the MRR transmission spectrum in Fig. 1 c). Generally, with reference to Fig. 1 a, depending on the wavelength of an input optical signal at the *in* or *add* port, and depending on the GST memory state (i.e. amorphization level), different fractions of the input light will be led to the *through* port, redirected to the *drop* port, or absorbed by the ring waveguide (which also comprises a PCM cell). The latter implies heating and increase in free carrier concentration of the resonator, with consequent volatile modification of the resonance properties, such as the resonant wavelengths. Furthermore, light absorption and consequent heating of the GST cell, if intense enough, triggers modifications to the non-volatile memory state. It should be also noticed that if light with the same wavelength enters through the two input ports at the same time, optical interference of overlapping beams will come into play as well. For more theoretical insight regarding this device, we refer to our previous work [1].

In order to evaluate the energy efficiency and contrast of memory operations (considering both GST amorphization and recrystallization), we sent a sequence of short optical pulses into the MRR input port, so as to change the solid-state phase of the GST cell. In particular, a single optical pulse of $10\,\mathrm{ns}$ duration was employed for GST amorphization, while for recrystallization we used a sequence of 100 pulses with the same duration and lower power, each separated by time intervals of $10\,\mathrm{ns}$, with total length of $2\,\mu\mathrm{s}$. We did so, instead of using the double-step pulse employed in [2], in order to demonstrate that the repetition of the same pulse shape used for amorphization can reverse the memory state as well. This is key to achieve a plastic behaviour of the node, whose memory states need to be fully accessible by employing the same input signal shape.

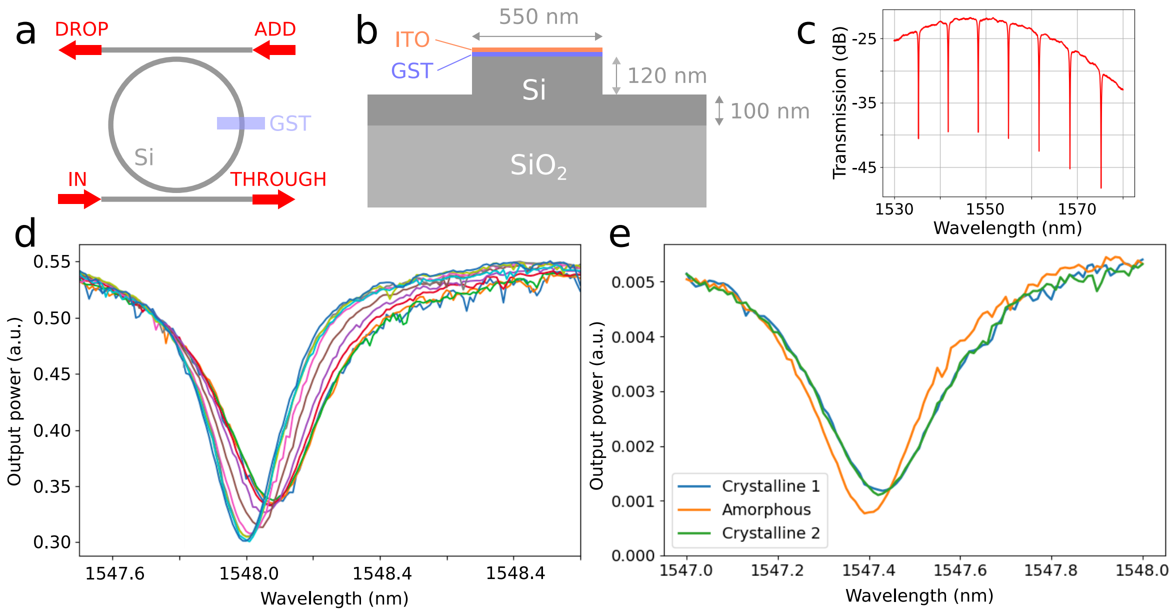

Figure 1: **All-optical plastic node. a** The considered plastic node, consisting of a silicon add-drop MRR with a PCM cell of $1\,\mu\mathrm{m}$ **b** PCM cell cross section. **c** Example of transmission spectrum of a silicon MRR (*through* port) showing multiple quasi-periodic resonance dips, measured using grating couplers. **d** Linear response of a plastic node (RR spectra showing resonance dips at the *through* output port) for different GST crystallinity levels, obtained by insertion of a single (amorphization) or multiple (crystallization) optical pulses. **e** Resonance spectrum of a plastic node, showing the non-volatile effect of single-pulse amorphization (from "Crystalline 1" to "Amorphous") and single-waveform recrystallization (from "Amorphous" to "Crystalline 2").

By suitably setting the power of the optical input pulses we obtained different GST amorphization levels, which can be considered as intermediate memory states, each presenting a different resonance dip in the acquired MRR spectrum at the *through* port (Fig. 1d). The chosen pulse wavelength is $0.06\,\mathrm{nm}$ larger than the resonance wavelength (corresponding to the center of the spectrum dip) when the GST is fully crystalline. In accordance to MRR theory, we ascribe the resonance dip changes in width and depth to variations of the GST cell absorption: a higher GST crystallization level implies a higher optical absorption, thus a larger width and a smaller depth of the resonance dip. Moreover, the GST solid-state phase also affects the effective refractive index of the corresponding waveguide segment, which in turns modifies the resonance wavelength. In particular, a larger crystalline fraction implies a larger effective refractive index and thus a larger resonance wavelength. Importantly, this effect further increases the achievable optical contrast due to different memory states, and therefore represents an additional advantage of employing a GST cell on a MRR rather than on a straight waveguide, whose transmission is much less affected by variations in effective refractive index. It should be stressed that we achieved a significantly higher optical contrast due to memory operations when experimentally investigating our plastic node compared to what we previously predicted through simulations [1] (probably because of inaccuracies in the material parameters used).

Let us now consider an example showing the maximum optical contrast, due to GST amorphization, that is achievable with a single pulse and is reversible using a single recrystallization waveform (comprising several pulses). In Fig. 1 e, we plotted the resonance spectra of a plastic node, corresponding to the following memory states: initial crystalline GST state (labelled as "Crystalline 1" in the legend); partially amorphized GST after the insertion of an amorphization pulse of around $14\,\mathrm{mW}$ peak power, conveying around $14\,\mathrm{nJ}$ of energy (labelled as "Amorphous" in the legend); return to initial crystalline state, after the insertion of a recrystallization waveform, consisting of pulses with around $1\,\mathrm{mW}$ peak power, conveying a total energy equal to around $1\,\mathrm{nJ}$ (labelled as "Crystalline 2" in the legend). In this case, a reversible optical contrast in the output power at 1547.4 nm greater than 40% is achieved. In comparison, to achieve a reversible optical contrast of 15% with a GST cell on a straight silicon waveguide (i.e. without the advantages of exploiting the MRR resonant behaviour), an amorphization pulse $100\,\mathrm{ns}$ long and with $1.6\,\mathrm{nJ}$ energy is required, and a recrystallization double-step pulse, $530\,\mathrm{ns}$ long and with $3.6\,\mathrm{nJ}$ energy [1]. Therefore, our plastic node shows the following improvements w.r.t. its straight waveguide counterpart: more than twice optical contrast; more than a factor 10 in amorphization energy efficiency; almost a factor 4 in recrystallization energy efficiency; a factor 10 in amorphization speed. The considered recrystallization operation, instead, is more than 3 times slower (although we did not try to maximize the speed), because it employs a sequence of single-step pulses, instead of double-step pulses. The fact that we do not need specially constructed pulses is key for the network plasticity property howere, since we want the same input shape to be able to change the memory states of the plastic nodes in both directions, allowing for a more flexible network adaptability.

2 Investigation of plastic self-adaptation properties

In this supplementary section we provide an expansion of the information given in Section 3 of the main text, regarding the plasticity introduced in the proposed photonic plastic recurrent resonator neural network (PPRRNN) by the MRRs with PCM. In particular, here we present histograms that summarize important properties of the plastic response over all the measurement sessions performed (listed in Table 2 in the main text).

We now aim to give an overview of how differently the network output is modified by the different input waveforms (i.e. due to plastic adaptation (PA) steps from different classes). In particular, by ‘network output’ we mean here the output feature vector extracted from the signals at different physical output ports of the PPRRNN. Namely, as explained in the main text, for a given input waveform (i.e. a sample from the machine learning perspective), we consider the energy of the last pulse in the corresponding waveforms at each output port. Thus, the considered output features vector has as many scalar elements as the number of physical output ports. To understand how the output features vector changes with different PA steps, we calculate the Pearson correlation coefficient between each pair of median variations of elements of the output feature vector, over the PA step sequence. E.g., looking at Fig. 2e in the main text, the correlation is calculated between the two vectors represented in the first and the second box on the first row, then between the two vectors represented in the first and the third box in the same row, and so on until all the pairs are covered. This is repeated for each measured PA step sequence. Obviously, here we consider only the measurement sessions with multiple output ports (first three in Table 2 in the main text). Then, we represent all these correlation values in a histogram (Fig. 2a). We can notice that, indeed, a significant portion of the investigated PA step pairs provide output feature variations with low correlations. In particular, 596 correlation coefficients of a total of 2746 are between -0.5 and 0.5 (this correlation range is arbitrarily chosen, to provide some intuitive insight). These low correlations are desired and show that the PPRRNN plastic response exhibits *richness*, as it can vary significantly depending on the input history. On the other hand, it should be noticed that a large number of pairs are highly anti-correlated, even exceeding the number of highly correlated pairs. This means that the variations due to a PA step are often reverted by another PA step in the same series. In other words, this shows that the plastic weights configuration in the PPRRNN can be often reset by a single PA step.

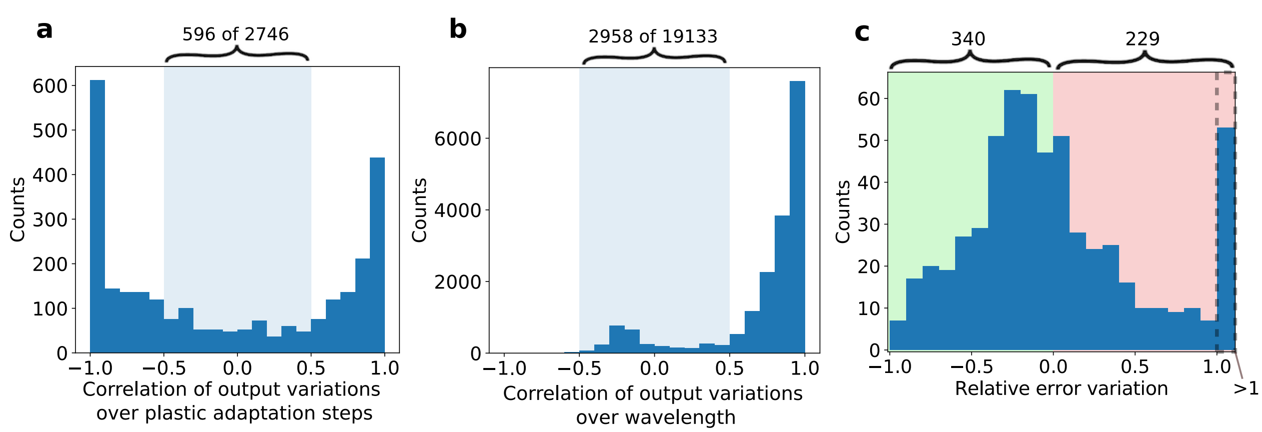

Figure 2: **Results of plasticity investigation. a, b** Histograms of the correlation coefficients between pairs of output feature variations, respectively for different PA steps and wavelengths. **c** Histogram of the error rate relative variations w.r.t. the initial error, in each sequence of PA steps.

We then performed a similar analysis by calculating the output feature variation correlation for different wavelength pairs, in the same measurement session and for a fixed PA step. E.g., looking at Fig. 2e in the main text, the correlation between the two vectors represented in the two boxes along the first column is estimated, the along the second column, and so on. Also in this case, we can see that a significant portion of variation pairs present low correlation (2958 of a total of 19133 have correlation between -0.5 and 0.5). This means that PA can present very different outcomes for different wavelengths of the input optical signal. On the other hand, it is not surprising that most of the pairs are highly correlated, since the minimum wavelength difference is only $0.005\,\mathrm{nm}$ and the maximum is $0.1\,\mathrm{nm}$, to be compared with the width (at half minimum) of a MRR resonance dip, which is larger than $0.2\,\mathrm{nm}$.

We now discuss our analysis of the machine learning (ML) classification results obtained for each measurement session, each wavelength and each PA step. Mainly, we are interested in seeing how different achieved plastic weights configurations result in different ML performance, i.e. in different performance of the PPRRNN when employed to provide useful data representation to be fed to a linear classifier. In addition to the three measurement sessions considered before in this section (first three in Table 2 in the main text), our analysis now comprises also measurement sessions where a single output port and a single wavelength are used, so to allow more (30) PA steps without exceedingly increasing the measurement duration (in Table 2 in the main text, from session 4 to 12). In order to provide an overall picture of the impact of the PA step in all the considered sequences, we show a histogram (Fig. 2c) of the error rate variations relative to the corresponding initial error rate value, due to each single PA step in all the measurement sessions. (This is different from Fig. 2g in the main text, which only considers the minimum over all PA steps, instead of every PA step individually.) It can be noticed that the value distribution is centered at negative relative error variations, showing that it was more frequent that a PA step resulted in a better ML performance w.r.t. the starting value, rather than the opposite. The counts in the negative relative error variation range are 340, against the 229 in the positive range. It should be considered that, since the plotted values are relative variations w.r.t. the initial value and they cannot be less than -1 (the error rate always being a positive number), the mean of the distribution is skewed towards positive values, which explains the highly populated tail consisting of values larger than 1.

References

[1] Alessio Lugnan, Santiago García-Cuevas Carrillo, C David Wright, and Peter Bienstman. Rigorous dynamic model of a silicon ring resonator with phase change material for a neuromorphic node. *Optics Express*, 30(14):25177–25194, 2022.

[2] Xuan Li, Nathan Youngblood, Zengguang Cheng, Santiago Garcia-Cuevas Carrillo, Emanuele Gemo, Wolfram HP Pernice, C David Wright, and Harish Bhaskaran. Experimental investigation of silicon and silicon nitride platforms for phase-change photonic in-memory computing. *Optica*, 7(3):218–225, 2020.